A Conformational Study of the Trisaccharide β-D-Glc*p*-(1→2)[β-D-Glc*p*-(1→3)]α-D-Glc*p*-OMe by NMR NOESY and TROESY Experiments, Computer Simulations, and X-Ray Crystal Structure Analysis

Torgny Rundlöf,[a] Lars Eriksson,[b] and Göran Widmalm*[a]

Abstract: Proton–proton cross-relaxation rates have been measured for the trisaccharide β-D-Glc*p*-(1→2)[β-D-Glc*p*-(1→3)]α-D-Glc*p*-OMe in D_2O as well as in D_2O/[D_6]DMSO 7:3 solution at 30 °C by means of one-dimensional NMR pulsed field gradient $^1H,^1H$ NOESY and TROESY experiments. Interatomic distances for the trisaccharide in D_2O were calculated from the cross-relaxation rates for two intraresidue and three interglycosidic proton pairs, using the isolated spin-pair approximation. In the solvent mixture one intraresidue and three interglycosidic distances were derived without the use of a specific molecular model. In this case the distances were calculated from the cross-relaxation rates in combination with "model-free" motional parameters previously derived from ^{13}C relaxation measurements. The proton–proton distances for interglycosidic pairs were compared with those averaged from Metropolis Monte Carlo and Langevin Dynamics simulations with the HSEA, PARM22, and CHEAT95 force fields. The crystal structure of the trisaccharide was solved by analysis of X-ray data. Interresidue proton pairs from the crystal structure and those observed by NMR experiments were similar. However, the corresponding proton–proton distances generated by computer simulations were longer. For the (1→2) linkage the glycosidic torsion angles of the crystal structure were found in a region of conformational space populated by all three force fields, whereas for the (1→3) linkage they occupied a region of low population density, as seen from the simulations.

Keywords: carbohydrates · molecular dynamics · molecular modeling · oligosaccharides · X-ray diffraction

Introduction

Carbohydrates found at cell surfaces have been shown to have important biological functions.[1] They often act as recognition molecules, mediating biological processes such as infection, inflammation, and cell–cell adhesion. Because of the importance of these functions in nature, the solution structures of carbohydrates have been intensively studied.[2, 3] Their polyhydroxylated surfaces make hydrogen bonding to the surrounding water important; as a result intramolecular hydrogen bonds, stabilizing the three-dimensional (3D) structure, become less common. Crystallization of these oligosaccharides may therefore be hard and the period of time necessary to obtain a crystal of useful size and quality will therefore be unpredictable. Thus, the 3D structure often has to be determined mainly by NMR spectroscopy in solution ($^3J_{C,H}$ and NOE) combined with molecular modeling techniques.[4] More recent methods applied to carbohydrates include off-resonance ROESY experiments[5] or measurement of residual dipolar couplings in oligosaccharides dissolved in aqueous dilute liquid-crystalline solutions.[6–8] Furthermore, the internal flexibility has to be taken into account; this complicates the determination of the 3D structure.[9] One way to investigate the internal dynamics is to bring the oligosaccharide outside the extreme narrowing regime, resulting in relaxation parameters that are dependent on the magnetic field strength.[10] However, the addition of dimethyl sulfoxide (DMSO) to a saccharide–water solution may influence the conformational properties of the solute. It is therefore important to address this issue, in particular to ask whether the DMSO/water solvent mixture is a relevant complement to water for studies of oligosaccharide conformation and dynamics. In the present study we combine NMR experiments with molecular modeling and the crystal structure to obtain a description of the conformation and dynamics of the trisaccharide β-D-Glc*p*-(1→2)[β-D-Glc*p*-(1→3)]α-D-Glc*p*-OMe, an oligosaccharide that acts as a model of the repeating unit of the exopolysaccharide from a strain of *Pedicoccus damnosus*.[11]

[a] Prof. Dr. G. Widmalm, Dr. T. Rundlöf
Department of Organic Chemistry
Stockholm University
106 91 Stockholm (Sweden)
Fax: (+46) 815-49-08
E-mail: gw@organ.su.se

[b] Dr. L. Eriksson
Department of Structural, Inorganic and Physical Chemistry
Arrhenius Laboratory, Stockholm University
106 91 Stockholm (Sweden)

0947-6539/01/0708-1750 $ 17.50+.50/0

Theory

For molecules in solution, proton relaxation is dominated by the dipole–dipole cross-relaxation between spins that are close in space. The strength of these interactions depends on the molecular dynamics, the internuclear distance(s), and the number of interacting spins. The cross-relaxation rate, σ, for the nuclear Overhauser effect (NOE)[12] and rotating-frame Overhauser effect (ROE)[13] can be expressed as combinations of spectral density functions taken at certain frequencies. The NOE cross-relaxation rate (σ_{NOE}) can be calculated from Equation (1).

$$\sigma_{NOE} = \tfrac{1}{4}(D_{HH})^2[6J(2\omega) - J(0)] \quad (1)$$

The corresponding equation for the ROE cross-relaxation rate (σ_{ROE}) is given in Equation (2).

$$\sigma_{ROE} = \tfrac{1}{4}(D_{HH})^2[2J(0) + 3J(\omega)] \quad (2)$$

Owing to problems with signals arising from TOCSY transfer[14] in ROE experiments, a modified multiple-pulse spin-lock has been proposed,[15] which efficiently suppresses such signals. The multiple-pulse or transverse ROE (TROE) cross-relaxation rate, σ_{TROE}, can be calculated as the mean of σ_{NOE} and σ_{ROE} and is described by Equation (3).

$$\sigma_{TROE} = \tfrac{1}{8}(D_{HH})^2[6J(2\omega) + 3J(\omega) + J(0)] \quad (3)$$

The dipolar coupling constant, $D_{HH} = (\mu_0/4\pi)\gamma^2\hbar r^{-3}$, is a measure of the strength of the dipolar interaction, where μ_0 is the permeability in vacuum, γ is the magnetogyric ratio for protons, $\hbar$ is Planck's constant divided by 2π, and r is the distance between interacting protons.

Unknown proton–proton distances, r_{ij}, between protons i and j can be obtained by the isolated spin-pair approximation[16, 17] (ISPA) by comparison of the cross-relaxation rate of the reference spin pair, σ_{ref}, with that of i and j, σ_{ij}, according to Equation (4).

$$r_{ij} = r_{ref}(\sigma_{ref}/\sigma_{ij})^{1/6} \quad (4)$$

The reference distance used, r_{ref}, should be chosen for protons residing in a well-defined part of the molecule.

Proton–proton distances can also be calculated from cross-relaxation rates[18] by the "model-free" approach,[19] provided that the motional parameters are known. In this approach the molecular motions are described by a slow global motion, τ_M, and a local motion, τ_e. Prerequisites are that the different motions are uncorrelated and that the molecule reorients isotropically. The restriction of the internal motion is described by a generalized order parameter, S^2, that adopts values between 0 and 1, with $S^2 = 1$ corresponding to a totally restricted internal motion. The model-free spectral density, $J(\omega)$, is expressed in Equation (5), where $\tau^{-1} = \tau_M^{-1} + \tau_e^{-1}$. If τ_e is much shorter than τ_M, the second term in Equation (5) makes a negligible contribution to the spectral density and the Equation can be truncated to give Equation (6).

$$J(\omega) = \frac{2}{5}\left(\frac{S^2\tau_M}{1 + \omega^2\tau_M^2} + \frac{(1-S^2)\tau}{1 + \omega^2\tau^2}\right) \quad (5)$$

$$J(\omega) = \frac{2}{5}\left(\frac{S^2\tau_M}{1 + \omega^2\tau_M^2}\right) \quad (6)$$

If the overall and internal correlation times are on similar timescales, they cannot be determined separately and an effective correlation time, τ_{eff}, for the molecular reorientation can be used, resulting in Equation (7).

$$J(\omega) = \frac{2}{5}\left(\frac{\tau_{eff}}{1 + \omega^2\tau_{eff}^2}\right) \quad (7)$$

With this expression, τ_{eff} can be calculated[20] from the NOE or TROE cross-relaxation rates [Equations (1) or (3)] and a known interproton distance obtained by the ISPA method. The effective correlation time can also be calculated from the ratio between σ_{NOE} and σ_{TROE}[21, 22] without a known reference distance, as shown in Equation (8).

$$\frac{\sigma_{NOE}}{\sigma_{TROE}} = \frac{10 + 42\omega^2\tau_{eff}^2 - 32\omega^4\tau_{eff}^4 - 32\omega^8\tau_{eff}^8}{10 + 63\omega^2\tau_{eff}^2 + 96\omega^4\tau_{eff}^4 + 16\omega^8\tau_{eff}^8} \quad (8)$$

Results and Discussion

Cross-relaxation measurements: The trisaccharide β-D-Glc*p*-(1→2)[β-D-Glc*p*-(1→3)]α-D-Glc*p*-OMe was investigated by NMR spectroscopy, specifically, ^{1}H 1D NOESY and 1D TROESY experiments, performed at 30 °C in D_2O and in the solvent mixture D_2O/[D_6]DMSO 7:3. The structure of the molecule and the notation for the different residues are shown in Scheme 1. Spectra were recorded at 600 MHz for the D_2O sample and at 500 and 600 MHz for the D_2O/[D_6]DMSO sample, using ten different mixing times from 30 to 1000 ms. Positive NOEs and TROEs were observed for the trisaccharide in D_2O, suggesting overall tumbling in or close to the extreme narrowing regime, where the spectral density function becomes less dependent on the magnetic field and an effective correlation time may be used. Spectra are exemplified in Figure 1, where selective inversion of the H1 resonance in the methyl α-glucoside residue (**g**) resulted in positive NOEs and TROEs of, inter alia, signals from H2 and H3 in the same residue, of the *O*-methyl group, and of H1 in the β-glucosyl residue (**g²**) substituting O2 of **g**. Inversion of the resonance from H1 in **g²** resulted in Overhauser effects of H1, H2, and H3 in **g**, of H3 and H5 in **g²**, and of H1 in the other β-glucosyl residue (**g³**). Inversion of H1 in **g³** gave NOE and

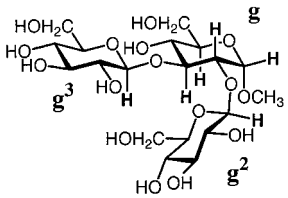

Scheme 1. Schematic representation of the trisaccharide β-D-Glc*p*-(1→2)[β-D-Glc*p*-(1→3)]α-D-Glc*p*-OMe showing the different sugar residues **g**, **g²**, and **g³**, and the protons (in bold) for which cross-relaxation rates have been measured.

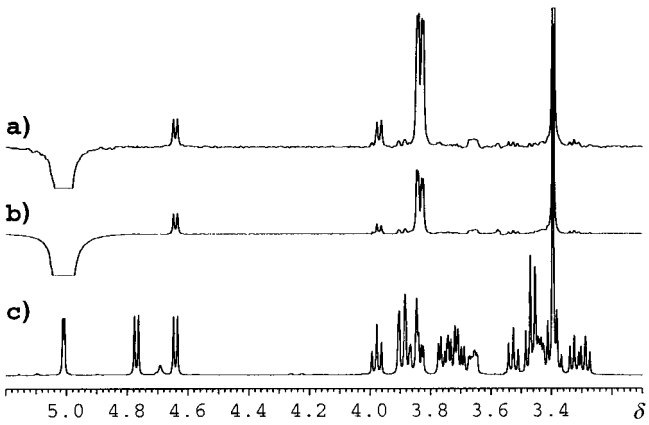

Figure 1. Spectra recorded at 600 MHz and 30 °C for the trisaccharide in D_2O. The a) TROE and b) NOE spectra are shown, recorded at mixing times of 700 ms, with selective excitation of H1 in the methyl glucoside (**g**) residue. Positive enhancements are observed, particularly for H2**g** (δ = 3.83) and H1**g²** (δ = 4.64). In c) the ordinary proton spectrum is shown.

TROE to H2, H3, and H4 in **g**, to H1 in **g²**, and intraresidually to H3 and H5. It was also possible to invert selectively H3 in **g**, cross-relaxing with H5 in the same residue and with H1 in **g²** and H1 in **g³**. For the measurements in D_2O/[D_6]DMSO, negative NOEs and positive TROEs were observed, demonstrating slower molecular tumbling outside the extreme narrowing regime. In this region, the NOE and TROE cross-relaxation rates should be field-dependent. Owing to spectral overlap, only the three anomeric protons could be selectively inverted in the solvent mixture; this inversion showed proton–proton interactions similar to those observed in D_2O.

Five and four proton–proton pairs were used for the calculation of cross-relaxation rates in D_2O and D_2O/[D_6]DMSO, respectively. The pairs were H1**g**–H2**g**, H1**g**–H1**g²**, H2**g**–H1**g²**, H3**g**–H1**g³**, and also H3**g**–H5**g** in the D_2O sample. For some pairs, cross-relaxation was detected at both the interacting protons, as shown in Table 1.

Table 1. Experimental cross-relaxation rates, σ_{NOE} and σ_{TROE}, at 303 K for the trisaccharide in D_2O/[D_6]DMSO 7:3 and in D_2O, calculated by second-order polynomial fits of normalized integrals.

Proton pair[a]	D_2O/[D_6]DMSO 500 MHz		D_2O/[D_6]DMSO 600 MHz		D_2O 600 MHz	
	σ_{NOE}	σ_{TROE}	σ_{NOE}	σ_{TROE}	σ_{NOE}	σ_{TROE}
1g–2g	−0.137	0.190	−0.141	0.177	0.037	0.118
1g–1g²[b]	−0.015	0.025	−0.018	0.023	0.008	0.026
1g–**1g²**[b]	−0.016	0.024	−0.020	0.024	0.007	0.022
2g–**1g²**	−0.191	0.316	−0.216	0.280	0.063	0.169
3g–5g	n.d.[c]	n.d.	n.d.	n.d.	0.029	0.067
3g–1g³	n.d.	n.d.	n.d.	n.d.	0.065	0.163
3g–**1g³**	−0.150	0.293	−0.167	0.265	0.062	0.155

[a] Excited proton in bold. [b] Linear fit of normalized integrals, for $\tau_{mix} <$ 100 ms. [c] n.d. = not determined.

NOE and TROE build-up curves can be used to calculate the cross-relaxation rates, determined as the slope of the initial linear regions. Therefore, measurements of normalized peak integrals at short mixing times are required, but these are problematic because of the low signal-to-noise ratios. The quality of the data in this study is exemplified by the NOE and TROE build-up curves for H1**g**–H2**g**, shown in Figure 2, with an expansion of the initial build-up region. Different methods have been developed to calculate the rates.[23] The cross-relaxation build-up versus the mixing time at sufficiently short mixing times can be fitted to a linear equation where the cross-relaxation rate is the slope of the fitted line. The build-up can also be fitted to a second-order polynomial; this permits peak amplitudes at slightly longer mixing times to be included in the fit. The latter method was used for all proton–proton interactions except one (see below), and proton cross-relaxation rates (σ_{NOE} and σ_{TROE}) were calculated by least-squares fits of the normalized integrals of the NOE or TROE peaks at different mixing times (see Experimental Section). For the fits of cross-relaxation rates in D_2O, only mixing times not longer than 300 ms (σ_{NOE}) and 450 ms (σ_{TROE}) were used in order to obtain the lowest possible errors in the calculated

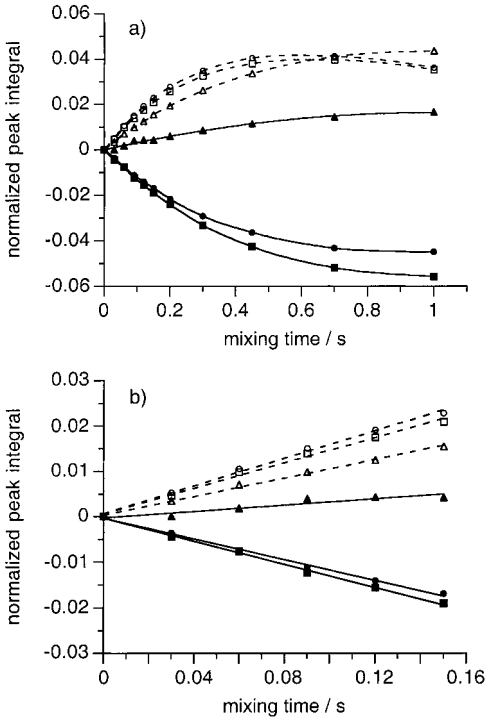

Figure 2. Experimental NOE (filled lines) and TROE (dotted lines) build-up curves for the intraresidue H1**g**–H2**g** spin pair, which is used as the reference interaction in the ISPA distance calculations. Shown in a) are TROEs in D_2O at 600 MHz (△), in D_2O/[D_6]DMSO at 500 MHz (○) and 600 MHz (□), and NOEs in D_2O at 600 MHz (▲), in D_2O/[D_6]DMSO at 500 MHz (●) and 600 MHz (■). In b) the corresponding initial linear regions of the build-up curves are shown. Note the negative NOE obtained with the D_2O/[D_6]DMSO sample.

cross-relaxation rates. Because of the larger magnitudes of the NOE and TROE cross-relaxation rates and more rapid total direct dipolar relaxation of the protons in the D_2O/[D_6]DMSO solution, only mixing times not longer than 150 ms were used for these fits.

For the H1**g**–H1**g²** interaction, indirect cross-relaxation via the H2**g** spin was possible. This was investigated by a full relaxation matrix analysis for two different conformers of the trisaccharide, namely, the crystal structure and the average conformation from the Metropolis Monte Carlo simulation (see below), using effective overall correlation times of 0.2 and 1 ns. It was found that for mixing times shorter than $\approx$100 ms the indirect effect was negligible. Similar results were obtained for both structures. Therefore, only mixing times $<$100 ms were used in linear fits of cross-relaxation rates for this dipolar interaction in both D_2O and the solvent mixture.

From the NOE spectra it was recognized that the motional behavior of the trisaccharide was different in D_2O and in the solvent mixture. The positive and negative NOEs, respectively, are a result of different tumbling correlation times for the trisaccharide. The viscosity of a H_2O/DMSO 7:3 solvent mixture is more than twice as high as that of H_2O.[24] Despite the slower tumbling rate it is reasonable to assume that the solute molecule behaves in a similar way as in water since the solvent mixture contains 70 molar % water and carbohydrates are hydrated in solution.[25, 26] The D_2O/[D_6]DMSO mixture

0947-6539/01/0708-1752 $ 17.50+.50/0 *Chem. Eur. J.* **2001**, *7*, No. 8

was recently used in studies of the ^{13}C NMR relaxation[27] and $^{1}H,^{13}C$ long-range coupling constant[28] of the trisaccharide.

The experimental cross-relaxation rates are reported in Table 1. In the solvent mixture, the intraresidue H1**g** – H2**g** and the interresidue H2**g** – H1**g**^{2} and H3**g** – H1**g**^{3} interactions showed fairly high absolute NOE and TROE cross-relaxation rates. The interaction between H1**g** and H1**g**^{2} was significantly weaker, with much lower cross-relaxation rates. The ratios between σ_{NOE} values at two different magnetic field strengths may give information on internal motions.[18, 29] If the intraresidue cross-relaxation rate ratio σ_{NOE} (600 MHz)/σ_{NOE} (500 MHz) differs from the observed interglycosidic ratios, this can be an indication of differences in internal motions between these two types. The ratio calculated for the intraresidue H1**g** – H2**g** rate was close to unity. The interglycosidic correlations H2**g** – H1**g**^{2} and H3**g** – H1**g**^{3} both had a ratio of 1.1, that is, only slightly different from the intraresidue ratio. Therefore, the dynamic parameters from the previous ^{13}C relaxation study[27] were judged appropriate for the analysis of proton – proton cross-relaxation data. Also, since the "dynamic equivalence" of different carbon – proton bond axes in a single carbohydrate ring was used,[30] one might expect this equivalence to extend to the intraring H1**g** – H2**g** axis, as has been shown for a disaccharide under similar experimental conditions.[18] In addition, the measurements at two magnetic fields yield independent data sets.

In D_2O, the NOE and TROE cross-relaxation rates were lower than those observed in the solvent mixture. The low σ_{NOE} values resulted in larger uncertainties compared to the measurements in D_2O/[D_6]DMSO. The TROE cross-relaxation rates were, however, larger than the NOE rates resulting in smaller errors for σ_{TROE}. The only exception again was the cross-relaxation between H1**g** and H1**g**^{2}, which showed small NOE and TROE cross-relaxation rates. Positive NOE cross-relaxation rates were observed for all interactions, indicating fast molecular tumbling in the vicinity of the extreme narrowing regime where the generalized order parameter and the overall correlation time cannot be separated from each other (see Theory). Effective correlation times τ_{eff} for the interproton correlations in water were calculated by taking the ratio of the measured cross-relaxation rates, $\sigma_{NOE}/\sigma_{TROE}$, and extracting a τ_{eff} with the aid of Equation (8). This resulted in an average $\tau_{eff} = 0.20 \pm 0.02$ ns, that is to say, the effective correlation times for the proton pairs are quite similar.

The experimental errors in the NOE and TROE measurements can be estimated from the results in Table 1, where the cross-relaxation rates are independently measured for both interacting protons, for example, H1**g** – H1**g**^{2}. Differences of up to $\pm 5\,\%$ from the average are observed for the σ_{NOE} and σ_{TROE} for this pair in the solvent mixture. In D_2O the differences are slightly larger as a result of the weaker interactions. However, a 5 % error in the cross-relaxation rate leads to a difference of $< 1\,\%$ in the determined distance. The other interactions in Table 1 are stronger than the H1**g** – H1**g**^{2} interaction, which should result in smaller errors in these measurements.

Computer simulations: In order to investigate how the internal motions influence the proton – proton distances in the trisaccharide, we performed 5 ns Langevin dynamics[31, 32] (LD) and 10^6 macro steps Metropolis Monte Carlo[33] (MMC) computer simulations. Three different force fields were used, namely PARM22 (MSI, San Diego, CA, USA) and CHEAT95[34] for the LD simulations, and the HSEA force field[35, 36] for the MMC simulations. The use of more than one force field facilitates the recognition of conformational trends,[37] although the choice of a particular force field may be difficult.[38] All simulations were performed in vacuum, but the LD simulations use random and frictional forces to mimic aqueous solution. CHEAT95 uses extended hydroxy groups devoid of hydroxy protons and a reduced partial charge of the oxygen atoms. Mainly, the $(1 \rightarrow 2)$ and $(1 \rightarrow 3)$ glycosidic linkages populated the *syn* conformations, having $\phi_H \approx 60^\circ$ and $\psi_H \approx 0^\circ$, except for the $(1 \rightarrow 2)$ linkage in the LD simulations using the PARM22 force field, which showed a large proportion of an *anti*-ϕ conformer with $\phi_H \approx 150^\circ$. The flexibility of the glycosidic linkages, determined as root-mean-square torsion angle fluctuations for ϕ_H and ψ_H, was in all cases largest for the LD simulations using the PARM22 force-field parameters and smallest for the MMC simulations. Scatter plots for the $(1 \rightarrow 2)$ and $(1 \rightarrow 3)$ linkages from the CHEAT95 simulations are shown in Figure 3. Effective

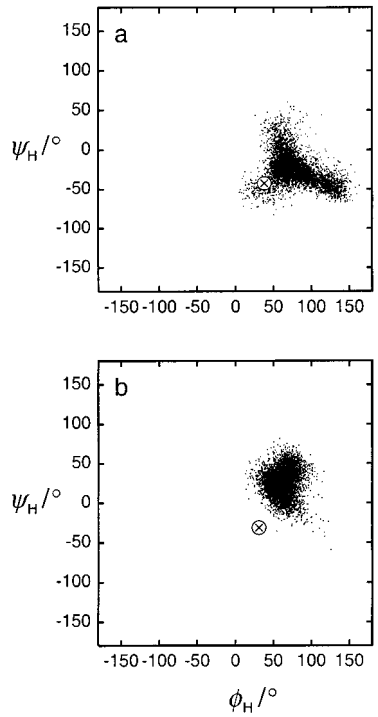

Figure 3. Scatter plots from the MMC simulations of a) the $(1 \rightarrow 2)$ linkage and b) the $(1 \rightarrow 3)$ linkage of the trisaccharide using the CHEAT95 force field. The crosses indicate the torsion angles found in the crystal structure.

(weighted) proton – proton distances were determined from the simulations, according to $(\langle r^{-3} \rangle^2)^{-1/6}$ averaging for conformational exchange processes faster than overall molecular rotational diffusion.[12, 39] The simulated interproton distances are reported in Table 2. Differences when $(\langle r^{-6} \rangle)^{-1/6}$ averaging was used (data not shown) were small and not critical for the outcome of this study. Furthermore, in a recent study on the

Table 2. Interproton distances r [Å] from simulations[a] using different force fields and from the X-ray crystal structure.

Proton pair	HSEA	PARM22	CHEAT95	Crystal
1g – 2g	2.38[b]	2.39	2.43	2.27
1g – 1g^2	3.68	4.31	3.79	3.03
2g – 1g^2	2.36	3.21	2.58	2.11
3g – 5g	2.61[b]	2.55	2.60	2.64
3g – 1g^3	2.47	2.51	2.68	2.26

[a] Averaged according to $r = (\langle r^{-3} \rangle^2)^{-1/6}$. [b] Fixed distance.

dynamics of a disaccharide,[40] the angular part of internuclear vectors in a molecule-fixed frame[41] contributing to the generalized order parameter was found to be negligible. In the present study, the effective intraresidue proton – proton distances in the **g** residue were found to be 2.39, 2.43, and 2.38 Å for H1 – H2 and 2.55, 2.60, and 2.61 Å for H3 – H5 by means of the PARM22, CHEAT95, and HSEA force fields, respectively. In simulations using HSEA these distances are fixed, since sugar residues are modeled as rigid units. Interresidue distances over the glycosidic linkages showed much more variation between force fields. For the two interactions between H1**g**^{2} and H1 and H2 in **g** the MMC simulations resulted in an effective $r = 3.68$ and 2.36 Å, respectively, but the LD simulations with PARM22 showed $r = 4.31$ and 3.21 Å, respectively. The latter distances result from the large amount of *anti*-ϕ conformer at this glycosidic linkage in the PARM22 simulations. The LD simulations with CHEAT95 showed somewhat longer interglycosidic distances than did the MMC simulations, a result that may be due to the increased flexibility observed with the former force field and/or differences in the average conformation at the glycosidic linkage.

Proton – proton distances: Cross-relaxation data for the trisaccharide in D_2O/[D_6]DMSO were interpreted by means of the model-free approach,[18, 19] whereas in D_2O the isolated spin-pair approximation[16, 17] (ISPA) was used. These procedures yielded experimental proton – proton distances for five proton pairs in D_2O and four pairs in D_2O/[D_6]DMSO, with the interproton distances reported in Table 3. Cross-relaxation rate averaging was performed prior to distance calculation for spin pairs for which rates were measured from both interacting protons.

Table 3. Experimental interproton distances r [Å] for the trisaccharide at 303 K, using the model-free approach[a] (D_2O/[D_6]DMSO 7:3) and ISPA[b] (D_2O).

Proton pair	D_2O/[D_6]DMSO				D_2O	
	500 MHz		600 MHz		600 MHz	
	r_{NOE}	r_{TROE}	r_{NOE}	r_{TROE}	r_{NOE}	r_{TROE}
1g – 2g	2.51	2.37	2.52	2.35	2.43[c]	2.43[c]
1g – 1g^2	3.33	3.28	3.27	3.25	3.18	3.16
2g – 1g^2	2.18	2.14	2.18	2.15	2.22	2.29
3g – 5g	n.d.[d]	n.d.	n.d.	n.d.	2.53	2.67
3g – 1g^3	2.30	2.17	2.30	2.17	2.22	2.31

[a] Calculated from Equation (5) and τ_M, S^2, and τ_e values from the sugar residue; interglycosidic distances are calculated with parameters from the terminal sugar residues. [b] Calculated from Equation (4). [c] Reference distance from LD simulation using the CHEAT95 force-field parameters. [d] n.d. = not determined.

In the solvent mixture, model-free motional parameters obtained by ^{13}C NMR relaxation measurements[27] were used to calculate interproton distances from the experimental cross-relaxation data, by Equations (1) or (3) and (5). For the intraresidue interaction H1**g** – H2**g**, an overall correlation time $\tau_M = 0.89$ ns, a generalized order parameter $S^2 = 0.84$, and an internal correlation time $\tau_e = 18$ ps were used, taken from the fits of ^{13}C NMR data of the **g** residue reported in Table 3 of the ^{13}C work.[27] From the NOE measurements interproton distances of 2.51 and 2.52 Å were obtained at 500 and 600 MHz, respectively. The TROE measurements resulted in shorter distances, 2.37 and 2.35 Å, respectively, at the two different magnetic fields. The simulation data give an average for the three force fields of 2.40 Å; in comparison, the distance obtained from the NOE measurements is longer, ≈2.51 Å, and that from the TROE measurements is shorter, ≈2.36 Å. Thus, the experimental determinations of the distance bracket the value calculated by computer simulations. Similar distances were obtained if the internal correlation time, $\tau_e =$ 18 ps, was omitted in the calculations. Taking into account the fact that no molecular model was used to derive the H1 – H2 distance, we find the small differences between experiment and simulation quite satisfactory. In a related study of another trisaccharide the intraresidue distance also showed good agreement to simulations, but in this case the model-free approach resulted in a slightly shorter distance when NOE data were used and a somewhat longer distance when TROE data were employed.[42] Subsequently, when ISPA is used (vide infra), a reverse relationship for r_{NOE} vs. r_{TROE} is obtained for the short trans-glycosidic distances. Therefore, the experimental differences should represent the accuracy of the data.

For the three interresidue interactions the motional parameters were taken from the terminal residues, that is, from **g**^{2} or **g**^{3}. These residues showed similar motional characteristics, with $\tau_M = 0.80$ and 0.81 ns, $S^2 = 0.70$ and 0.72, and $\tau_e = 57$ and 58 ps for **g**^{2} and **g**^{3}, respectively. For the interglycosidic interactions, the distances obtained by NOE measurements were in all cases longer than those obtained by TROE measurements. However, the differences were smaller than those observed for the intraresidue distance between H1**g** and H2**g**. When the interglycosidic distances were calculated with the ^{13}C model-free motional parameters of the **g** residue, longer distances were obtained. For example, the distances calculated from σ_{NOE} for H1**g** – H1**g**^{2} at both magnetic field strengths were ≈3.5 Å, compared with ≈3.3 Å if the motional parameters of the **g**^{2} residue were used. For the distances derived from σ_{TROE} the differences were much smaller ($\Delta r <$ 0.1 Å). Furthermore, in our distance calculations small differences in the input of S^2 did not alter the outcome of the interproton distance to any great extent (<1%), provided that τ_M and τ_e were not changed.

Interproton distances were also calculated from the NOE and TROE cross-relaxation rates measured in D_2O solution, with the isolated spin-pair approximation (ISPA) method. A certain cross-relaxation rate is compared with the rate obtained for a reference interaction having a known, fixed

0947-6539/01/0708-1754 $ 17.50+.50/0 *Chem. Eur. J.* **2001**, *7*, No. 8

distance in the molecule. From Equation (4) the unknown interproton distance of the spin pair of interest can be determined. Two possible intraresidue reference distances were available, H1**g** – H2**g** and H3**g** – H5**g**. The former proton pair was used, since its cross-relaxation rates were larger and the experimental errors smaller. NMR-derived distances are time-averaged. Therefore, an averaged reference distance should be used, obtained from, say, a molecular dynamics simulation. The average ϕ_H and ψ_H angles for the $(1\rightarrow2)$ linkage in the CHEAT95 LD simulation agreed better with those of the crystal structure than did those in the PARM22 LD simulation. Therefore, the time-averaged distance derived for H1**g** – H2**g** from the CHEAT95 LD simulation, calculated as $r=(\langle r^{-3}\rangle^2)^{-1/6}=2.43$ Å, was used as the reference distance in the ISPA distance calculations. A test of the precision of the reference distance employed was obtained by calculating the distances from the measured cross-relaxation rates of the H3**g** – H5**g** interaction. Both the NOE- and TROE-derived distances, $r=2.53$ and 2.67 Å, respectively, were in good agreement with those obtained from the simulations, for example 2.60 Å for CHEAT95 (Table 2). Interglycosidic distances were calculated for H1**g** – H1**g²**, H2**g** – H1**g²**, and H3**g** – H1**g³**. For the first proton pair, fairly long distances were obtained, $r=3.18$ and 3.16 Å from the NOE and TROE data, respectively. For the two latter proton pairs the NOE-derived distances were somewhat shorter than those obtained by TROE measurements, taking values of $\approx$2.2 and $\approx$2.3 Å, respectively. Such short interglycosidic proton – proton distances indicate ϕ_H and ψ_H values in the vicinity of 0°. A large proportion of an *anti* conformation for either ϕ_H or ψ_H should result in a longer distance. Therefore, these glycosidic linkages should mainly adopt *syn* conformations. Furthermore, an *anti* conformation would have resulted in an even longer H1**g** – H1**g²** distance, which was also observed from the LD simulations using the PARM22 force field.

Both *anti*-ϕ[43] and *anti*-ψ[44] conformers have been shown to exist at glycosidic linkages in oligosaccharides. However, quantifying the population of an *anti* conformation may be complicated owing to, inter alia, the influence of spin diffusion.[45] A remedy in such a case would be the elimination of intervening spins. The synthesis of a specifically deuterated methyl α-cellobioside was recently reported[46] and a conformational analysis of the disaccharide is presently being carried out.

Comparisons of the distances obtained from the cross-relaxation measurements in D_2O/[D_6]DMSO with those in D_2O, reported in Table 3, revealed fairly similar interglycosidic proton – proton distances. This observation indicates that the average conformation of the trisaccharide in the solvent mixture is similar to that in water solution. Also, we have recently noted that the water:DMSO ratio was significantly higher ($\approx$5:1) in the first solvent shell around a disaccharide than in the bulk solvent mixture (3:1), as deduced by MD simulations.[47]

Crystal structure: The solid-state structure of the trisaccharide was obtained by X-ray crystallography; the molecular structure of the trisaccharide is shown in Figure 4. The glycosidic torsion angles describe an all-*syn* conformation, where the anomeric proton and the proton at the glycosyloxylated carbon are close in space. In the present case for ease of comparison the glycosidic torsion angles are discussed with respect to a hydrogen atom even though the hydrogen atoms were placed geometrically on the basis of the heavy atom positions. These torsion angles are: for the $(1\rightarrow2)$ linkage given by $\phi_H=40°$ and $\psi_H=-42°$, for the $(1\rightarrow3)$ linkage $\phi_H=32°$ and $\psi_H=-29°$, and for the *O*-methyl group $\phi_H=-47°$. The conformation of the hydroxymethyl groups is *gg* for $\omega=-64°$ and $\omega_2=-64°$, whereas $\omega_3=54°$, that is, a *gt* conformation. The packing in the *ac* plane is shown in Figure 5. No

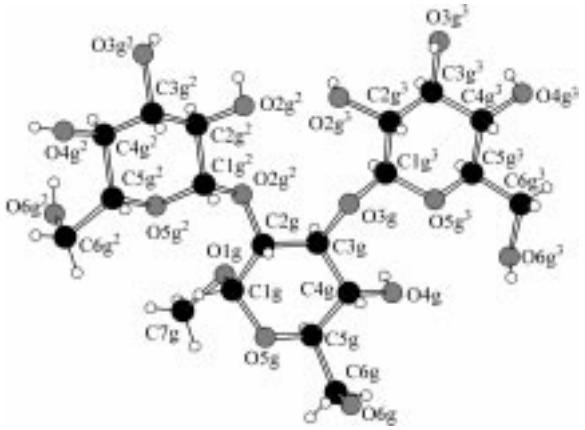

Figure 4. Molecular structure of the trisaccharide in the solid state as determined by X-ray crystallography, also showing the atomic numbering.

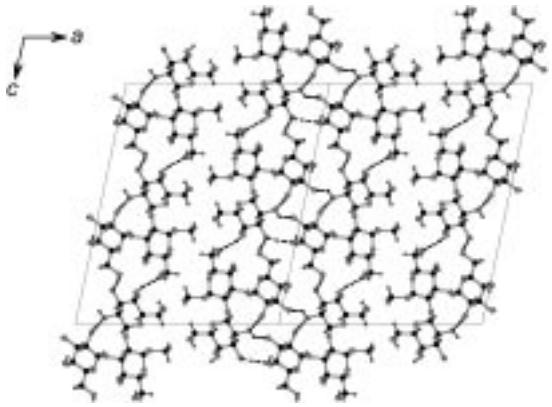

Figure 5. Crystal packing of the trisaccharide in the *ac* plane with two unit cells of four molecules each. Selected hydrogen bonds are shown by dashed lines. Note the hydrophilic vs. the hydrophobic regions. Oxygen atoms are shown in grey, carbons in black and hydrogens in white.

definite hydrogen-bonding scheme can be proposed owing to the difficulty in locating hydrogens from the X-ray diffraction data, but the close oxygen contacts continue both along the *c* axis and the *b* axis giving "sheets" of hydrogen-bonded molecules that pack together as a result of hydrophobic interactions between the blocks. One easily detected hydrogen-bond chain runs between the molecules in the *b* direction (Figure 6). The chain consists of O4**g** – C4**g** – C5**g** – C6**g** – O6**g** of each molecule and O4**g** connected to O6**g**$(x,y-1,z)$ in an infinite chain along the *b* axis. The intermolecular hydrogen-bond distance O4**g** – O6**g**$(x,y-1,z)$ is 2.97 Å. It is suggested

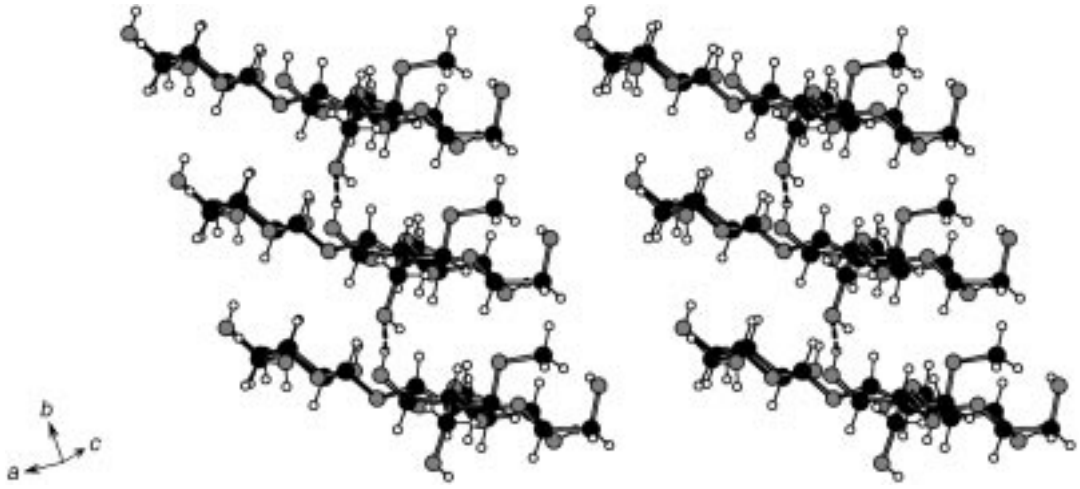

Figure 6. Stereoview of the packing along the *b* direction, with a distinct hydrogen bond chain (dashed) from O4**g** in one molecule to O6**g** in another.

that O4**g** acts as a donor and O6**g** as an acceptor where HO4**g** makes the hydrogen bond.

The $^{1}H,^{13}C$ heteronuclear coupling constants corresponding to the glycosidic torsion angles measured from the crystal structure were calculated by a Karplus relationship.[48] Values of 3.3 and 4.2 Hz were obtained from ϕ_H of the $(1\rightarrow2)$ and $(1\rightarrow3)$ linkages, respectively, and 3.0 and 4.4 Hz were obtained from ψ_H of those linkages. Recently, we measured interglycosidic long-range proton–carbon coupling constants for the trisaccharide in D_2O/[D_6]DMSO and D_2O.[28] Flexibility-averaged coupling constants were also calculated from LD and MMC simulations. The coupling constants measured from NMR spectra in the solvent mixture and in D_2O were 3.7–4.0 Hz (ϕ_H) and 4.5–4.9 Hz (ψ_H). These values agree with those calculated from the crystal structure in all cases but one, namely, for the coupling related to ψ for the $(1\rightarrow2)$ linkage ($\Delta^3J_{C,H} > 1.5$ Hz). In comparison, in the ^{13}C relaxation studies[27] and glycosylation shift analysis[49] no or only small differences in flexibility between the $(1\rightarrow2)$ and $(1\rightarrow3)$ linkages were observed, results which are further strengthened in this study by the similar interglycosidic distances obtained for these linkages in D_2O and the solvent mixture.

The intra- and interresidue proton–proton distances derived from the NOE and TROE experiments were also measured from the crystal structure, as reported in Table 2. The overall agreement between the experimentally determined interproton distances is quite high, indicating that the crystal structure of the trisaccharide is quite similar to the average conformations in solution. Four of the five distances were shorter in the solid state, and one, H3**g**–H5**g**, was close to those obtained from the simulations. Distances calculated from the MMC simulations using the HSEA force field agreed best with those measured from the crystal structure, with the interglycosidic distances for the protons at the linkage positions ≈0.2 Å longer.

Conclusion

The trisaccharide in this study was investigated by solution-state NMR spectroscopy, which, using either model-free motional parameters or a dynamically averaged molecular model with an internal reference distance, gave proton–proton distances for comparison with computer simulations. The trans-glycosidic distances from simulations were longer than those from NMR experiments, whereas the distances obtained from the crystal structure determined in this work agreed better with NMR data. From H1**g**^{2} two interresidue correlations were observed, one with a somewhat longer and the other a somewhat shorter distance in the solvent mixture than in D_2O. These small differences indicate that only minor conformational changes exist between the solvent mixture and D_2O, despite the limited number of cross-relaxing interglycosidic spin pairs. The present work, which contains, inter alia, high-quality Overhauser effect NMR data, reveals the importance of further tuning of molecular mechanics force fields for use with computer simulations in order to describe flexibility and dynamics of more complex molecular systems. Furthermore, we have shown that the combination of ^{13}C NMR relaxation studies, yielding the motional properties, and $^{1}H,^{1}H$ NOESY or TROESY experiments is a general method and an excellent way to approach the conformational problems of biomolecules.

Experimental Section

General: The synthesis of the trisaccharide β-D-Glc*p*-$(1\rightarrow2)$[β-D-Glc*p*-$(1\rightarrow3)$]α-D-Glc*p*-OMe has already been described.[49] NMR samples were prepared in 5 mm NMR tubes as 0.1M solutions of the trisaccharide in D_2O or D_2O/[D_6]DMSO in a 7:3 molar ratio. The solutions were treated with CHELEX 100 in order to remove any paramagnetic ions present, and the NMR tubes were sealed under vacuum after three freeze–pump–thaw cycles. The ^{1}H NMR chemical shifts in D_2O were assigned previously,[49] and the differences upon changing to the D_2O/[D_6]DMSO solvent mixture were checked by two-dimensional $^{1}H,^{1}H$ and $^{1}H,^{13}C$ correlation experiments.

Spectra were recorded at 30 °C on Varian Inova 500 and Inova 600 spectrometers operating at 500 and 600 MHz, respectively, equipped with triple-resonance pulsed field gradient HCX probes. Spectra recorded on another Varian Inova 600 spectrometer were used to check the accuracy of the measurements. These data were similar but not used in the calculations of the reported cross-relaxation rates.

Trisaccharide crystals were obtained from acetonitrile/water/methanol in the proportions 50:2:1.

0947-6539/01/0708-1756 $ 17.50+.50/0 *Chem. Eur. J.* **2001**, *7*, No. 8

Cross-relaxation measurements: Proton–proton cross-relaxation rates were measured in one-dimensional DPFGSE-NOESY experiments[50, 51] (σ_{NOE}) and DPFGSE-TROESY experiments[15, 52] (σ_{TROE}). Selective excitations at the frequency of well-resolved signals were enabled using i-Snob-2 shaped pulses[53] of 40 or 50 ms duration. The gradient durations in the initial DPFGSE part were 1 ms and the strengths 0.9 and 2.4 G cm^{-1}, respectively, in D_2O, and 13.9 and 6.0 G cm^{-1}, respectively, in D_2O/[D_6]DMSO. In the subsequent NOESY part of the pulse sequence, four gradients of 1 ms duration were run in pairs with strengths 1.2 and 1.6 G cm^{-1}, respectively, with a 2 ms hyperbolic secant inversion pulse[54] inserted between the gradients in each pair. All other pulses were hard and of short duration, <8 μs for a 90° pulse. For the TROE experiment the DPFGSE part was followed by a TROESY spin lock[14] with $\gamma B_1/2\pi =$ 2.8 kHz.

Spectra were recorded with a spectral width of 2000 Hz and 16k complex points; 196–512 transients were sampled at each mixing time. For the D_2O sample, measurements were performed at 600 MHz using selective excitations at four frequencies. For the D_2O/[D_6]DMSO sample, resonances at three frequencies were selectively excited at both 500 and 600 MHz. The total relaxation delay (acquisition + delay) between transients was 12 s (D_2O), 12 s (D_2O/[D_6]DMSO, 500 MHz), and 14 s (D_2O/[D_6]DMSO, 600 MHz), i.e., always $>5\,T_1$. Ten different cross-relaxation delays (mixing times) of 0.03, 0.06, 0.09, 0.12, 0.15, 0.2, 0.3, 0.45, 0.7, and 1.0 s were used.

Prior to Fourier transformation, the FIDs were zero-filled once and multiplied with a 1 Hz exponential line-broadening factor. Spectra were baseline-corrected with a first-order correction, and integrated using the same integration limits at all mixing times.

Integrated auto-peaks were fitted to an exponential decaying function, and normalized cross-relaxation integrals were obtained by division of the measured integrals by the extrapolated auto-peak value at zero mixing time. The regression coefficients in the fits were $R>0.9993$ for the auto-peaks in D_2O, except for the NOE H3**g** excitation which had $R>0.997$. For the auto-peak curves in D_2O/[D_6]DMSO $R>0.9996$ was obtained.

Cross-relaxation build-up curves were obtained from the normalized integrals at different mixing times, and the rates were calculated by fitting a second-order polynomial using mixing times not longer than 450 ms and 300 ms for σ_{NOE} and σ_{TROE} in D_2O, respectively, and 150 ms for σ_{NOE} and σ_{TROE} in D_2O/[D_6]DMSO. Mixing times were discarded stepwise, starting from 1000 ms, until the best value of the regression coefficient was obtained. The errors in the least-squares fits, expressed using the regression coefficient, were found to be $R>0.994$ in all cases, except for the σ_{NOE} of H1**g**–H2**g** in D_2O, which had $R>0.989$. For H1**g**–H1**g²** only mixing times shorter than 100 ms were used in linear fits of peak integrals, owing to a possible three-spin effect, investigated using the noesim program.[32] In these linear fits, $R>0.989$ was obtained, except for σ_{NOE} in D_2O/[D_6]DMSO and σ_{TROE} in D_2O, for which R was >0.975.

Computer simulations: Langevin dynamics (LD) and Metropolis Monte Carlo (MMC) simulations were performed at 300 K. The PARM22 (MSI, San Diego, CA, USA) and CHEAT95 force field[34] parameters implemented in the CHARMM[55] program were used for the 5 ns LD simulations, using dielectric constants $\varepsilon=1$ and $\varepsilon=r$ (distance dependent) for the two force fields, respectively. The time step was 1 fs, data were sampled every 0.1 ps, and the Langevin collision frequency for carbon and oxygen atoms was 50 ps^{-1}. MMC simulations,[33] using the HSEA force field[35, 36] and the GEGOP program,[56] were performed with 10^6 macro steps, a maximum ϕ_H and ψ_H torsion angle change of 20° in each step and a total acceptance ratio of 37%. The glycosidic torsion angles are defined as ϕ_H (H1′-C1′-OX-CX) and ψ_H (C1′-OX-CX-HX), with X as the linkage position and the atoms of the glucosyl group primed. The torsion angles of the hydroxymethyl groups are defined as ω (O5-C5-C6-O6) with an index where appropriate.

X-ray crystal structure analysis: Single-crystal X-ray diffraction data were collected with a STOE IPDS diffractometer. The structure was solved by direct methods with SHELXS97.[57] Most of the non-hydrogen atoms were located in the initial electron density map and the rest of them in subsequent difference Fourier maps. All hydrogen atoms were geometrically placed and allowed to ride on the carbon or oxygen atom to which they were connected. The model was refined by full-matrix least-square calculations with SHELXL97.[58] Isotropic displacement parameters were used for all atoms because of the small amount of significant data. As a result of the small crystal size ($10\times10\times100$ μm), most reflections were weak and the final figure of merit is rather high. A summary of the crystallographic data is found in Table 4. Crystallographic data (excluding structure factors) for the structure reported in this paper have been deposited with the Cambridge Crystallographic Data Centre as supplementary publication no. CCDC-137451. Copies of the data can be obtained free of charge on application to The Director, CCDC, 12 Union Road, Cambridge CB2 1EZ, UK (Fax: (+44) 1223-336-033; e-mail: deposit@ccdc.cam.ac.uk).

Table 4. Crystal data and data collection parameters.

formula	$C_{38}H_{68}O_{32}$
M [g mol^{-1}]	1036.92
space group	$A2$ (5)
a [Å]	19.69(1)
b [Å]	5.11(1)
c [Å]	23.80(1)
β [°]	102.00(5)
volume [Å^3]	2344(5)
Z	2
ρ_{calcd} [g cm^{-3}]	1.469
radiation	$Mo_{K\alpha}$ ($\lambda\approx0.7107$ Å)
μ [mm^{-1}]	0.130
Θ_{max} [°]	23.92
index ranges	$-22\le h\le22$; $-5\le k\le5$; $-26\le l\le26$
measured reflns	7384
unique reflns	3594
observed reflns [$I\ge2\sigma(I)$]	899
parameters	152
refinement method	full-matrix least-square on F^2, $w=1/\sigma^2(F_o^2)$
GoF	1.93
$wR2$[a]	0.1997 (observed data), 0.2603 (all data)
$R1$[b]	0.1103 (observed data), 0.3788(all data)
final diff Four. map [e Å^{-3}]	min: −0.593, max: 0.612

[a] $wR2=(\Sigma w(F_o^2-F_c^2)/\Sigma wF_o^2)^{1/2}$. [b] $R1=\Sigma\,||F_o|-|F_c||/\Sigma\,|F_o|$.

Acknowledgements

The Swedish Natural Science Research Council is acknowledged for financial support. The Swedish NMR Centre, Gothenburg, is thanked for providing access to the Inova 500 and 600 NMR spectrometers. We are grateful to Dr. Toshi Nishida for valuable discussions.

[1] R. A. Dwek, *Chem. Rev.* **1996**, *96*, 683–720.
[2] T. Peters, B. M. Pinto, *Curr. Opin. Struct. Biol.* **1996**, *6*, 710–720.
[3] A. Imberty, *Curr. Opin. Struct. Biol.* **1997**, *7*, 617–623.
[4] G. Widmalm in *Carbohydrate Chemistry* (Ed.: G.-J. Boons), Blackie Academic & Professional, London, **1998**, pp. 448–502.
[5] P. Berthault, N. Birlirakis, G. Rubinstenn, P. Sinaÿ, H. Desvaux, *J. Biomol. NMR* **1996**, *8*, 23–35.
[6] T. Rundlöf, C. Landersjö, K. Lycknert, A. Maliniak, G. Widmalm, *Magn. Reson. Chem.* **1998**, *36*, 773–776.
[7] P. J. Bolon, J. H. Prestegard, *J. Am. Chem. Soc.* **1998**, *120*, 9366–9367.
[8] G. R. Kiddle, S. W. Homans, *FEBS Lett.* **1998**, *436*, 128–130.
[9] A. Poveda, J. L. Asiensio, M. Martín-Pastor, J. Jiménez-Barbero, *J. Biomol. NMR* **1997**, *10*, 29–43.
[10] J. Kowalewski, L. Mäler, G. Widmalm, *J. Mol. Liq.* **1998**, *78*, 255–261.
[11] M. T. Duenas-Chasco, M. A. Rodriguez-Carvajal, P. T. Mateo, G. Franco-Rodriguez, J. L. Espartero, A. Irastorza-Iribas, A. M. Gil-Serrano, *Carbohydr. Res.* **1997**, *303*, 453–458.
[12] D. Neuhaus, M. Williamson, *The Nuclear Overhauser Effect in Structural and Conformational Analysis*, VCH, New York, **1989**.
[13] A. A. Bothner-By, R. L. Stephens, J.-M. Lee, C. D. Warren, R. W. Jeanloz, *J. Am. Chem. Soc.* **1984**, *106*, 811–813.
[14] T.-L. Hwang, A. J. Shaka, *J. Magn. Reson. B* **1993**, *102*, 155–165.
[15] T.-L. Hwang, A. J. Shaka, *J. Am. Chem. Soc.* **1992**, *114*, 3157–3159.

[16] J. W. Keepers, T. L. James, *J. Magn. Reson.* **1984**, *57*, 404 – 426.
[17] P. D. Thomas, V. J. Basus, T. L. James, *Proc. Natl. Acad. Sci. USA* **1991**, *88*, 1237 – 1241.
[18] L. Mäler, G. Widmalm, J. Kowalewski, *J. Phys. Chem.* **1996**, *100*, 17103 – 17110.
[19] G. Lipari, A. Szabo, *J. Am. Chem. Soc.* **1982**, *104*, 4546 – 4559.
[20] J. P. M. Lommerse, L. M. J. Kroon-Batenburg, J. Kroon, J. P. Kamerling, J. F. G. Vliegenthart, *J. Biomol. NMR* **1995**, *5*, 79 – 94.
[21] D. G. Davis, *J. Am. Chem. Soc.* **1987**, *109*, 3471 – 3472.
[22] A. Poveda, J. L. Aseniso, M. Martín-Pastor, J. Jiménez-Barbero, *Carbohydr. Res.* **1997**, *300*, 3 – 10.
[23] J. D. Baleja, J. Moult, B. D. Sykes, *J. Magn. Reson.* **1990**, *87*, 375 – 384.
[24] J. M. G. Cowie, P. M. Toporowski, *Can. J. Chem.* **1961**, *39*, 2240 – 2243.
[25] S. B. Engelsen, S. Pérez, *Carbohydr. Res.* **1996**, *292*, 21 – 38.
[26] S. E. Harding, *Prog. Biophys. Molec. Biol.* **1997**, *68*, 207 – 262.
[27] A. Kjellberg, T. Rundlöf, J. Kowalewski, G. Widmalm, *J. Phys. Chem. B* **1998**, *102*, 1013 – 1020.
[28] T. Rundlöf, A. Kjellberg, C. Damberg, T. Nishida, G. Widmalm, *Magn. Reson. Chem.* **1998**, *36*, 839 – 847.
[29] M. Hricovíni, R. N. Shah, J. P. Carver, *Biochemistry* **1992**, *31*, 10018 – 10023.
[30] J. Kowalewski, G. Widmalm, *J. Phys. Chem.* **1996**, *100*, 28 – 34.
[31] R. W. Pastor, in *The Molecular Dynamics of Liquid Crystals* (Eds.: G. R. Luckhurst, C. A. Veracini), Kluwer Academic, Dordrecht, **1994**, pp. 85 – 138.
[32] B. J. Hardy, W. Egan, G. Widmalm, *Int. J. Biol. Macromol.* **1995**, *17*, 149 – 160.
[33] T. Peters, B. Meyer, R. Stuike-Prill, R. Somorjai, J.-R. Brisson, *Carbohydr. Res.* **1993**, *238*, 49 – 73.
[34] M. L. C. E. Kouwijzer, P. D. J. Groothenhuis, *J. Phys. Chem.* **1995**, *99*, 13426 – 13436.
[35] R. U. Lemieux, K. Bock, L. T. J. Delbaere, S. Koto, V. S. Rao, *Can. J. Chem.* **1980**, *58*, 631 – 653.
[36] H. Thøgersen, R. U. Lemieux, K. Bock, B. Meyer, *Can. J. Chem.* **1982**, *60*, 44 – 57.
[37] C. Landersjö, C. Höög, A. Maliniak, G. Widmalm, *J. Phys. Chem. B* **2000**, *104*, 5618 – 5624.
[38] S. Pérez, A. Imberty, S. B. Engelsen, J. Gruza, K. Mazeau, J. Jiménez-Barbero, A. Poveda, J. F. Espinosa, B. P. van Eyck, G. Johnson, A. D. French, M. L. C. E. Kouwijzer, P. D. J. Grootenuis, A. Bernardi, L. Raimondi, H. Senderowitz, V. Durier, G. Vergoten, K. Rasmussen, *Carbohydr. Res.* **1998**, *314*, 141 – 155.
[39] J. Tropp, *J. Chem. Phys.* **1980**, *72*, 6035 – 6043.
[40] A. Vishnyakov, G. Widmalm, J. Kowalewski, A. Laaksonen, *J. Am. Chem. Soc.* **1999**, *121*, 5403 – 5412.
[41] R. Brüschweiler, B. Roux, M. Blackledge, C. Griesinger, M. Karplus, R. R. Ernst, *J. Am. Chem. Soc.* **1992**, *114*, 2289 – 2302.
[42] C. Höög, C. Landersjö, G. Widmalm, *Chem. Eur. J.*, **2001**, in press.
[43] C. Landersjö, R. Stenutz, G. Widmalm, *J. Am. Chem. Soc.* **1997**, *119*, 8695 – 8698.
[44] J. Dabrowski, T. Kozár, H. Grosskurth, N. E. Nifant'ev, *J. Am. Chem. Soc.* **1995**, *117*, 5534 – 5539.
[45] B. J. Hardy, A. Gutierrez, K. Lesiak, E. Seidl, G. Widmalm, *J. Phys. Chem.* **1996**, *100*, 9187 – 9192.
[46] P. Söderman, G. Widmalm, *J. Org. Chem.* **1999**, *64*, 4199 – 4200.
[47] A. Vishnyakov, G. Widmalm, A. Laaksonen, *Angew. Chem.* **2000**, *112*, 144 – 146; *Angew. Chem. Int. Ed.* **2000**, *39*, 140 – 142.
[48] I. Tvaroska, M. Hricovíni, E. Petráková, *Carbohydr. Res.* **1989**, *189*, 359 – 362.
[49] P.-E. Jansson, A. Kjellberg, T. Rundlöf, G. Widmalm, *J. Chem. Soc. Perkin Trans. 2* **1996**, 33 – 37.
[50] K. Stott, J. Stonehouse, J. Keeler, T.-L. Hwang, A. J. Shaka, *J. Am. Chem. Soc.* **1995**, *117*, 4199 – 4200.
[51] K. Stott, J. Keeler, Q. N. Van, A. J. Shaka, *J. Magn. Reson.* **1997**, *125*, 302 – 324.
[52] A. Kjellberg, G. Widmalm, *Biopolymers* **1999**, *50*, 391 – 399.
[53] E. Kupce, J. Boyd, I. D. Campbell, *J. Magn. Reson. B* **1995**, *106*, 300 – 303.
[54] M. S. Silver, R. I. Joseph, D. I. Hoult, *J. Magn. Reson.* **1984**, *59*, 347 – 351.
[55] B. R. Brooks, R. E. Bruccoleri, B. D. Olafson, D. J. States, S. Swaminathan, M. Karplus, *J. Comput. Chem.* **1983**, *4*, 187 – 217.
[56] R. Stuike-Prill, B. Meyer, *Eur. J. Biochem.* **1990**, *194*, 903 – 919.
[57] G. M. Sheldrick, *Acta Crystallogr.* **1990**, *A46*, 467 – 473.
[58] G. M. Sheldrick, SHELXL 97, Program for the Refinement of Crystal Structures, University of Göttingen, Germany, **1997**.

Received: September 25, 2000 [F2749]

  0947-6539/01/0708-1758 $ 17.50+.50/0